LAWRENCE
LIVERMORE
NATIONAL
LABORATORY

UCRL-CONF-216444

Patch-based Adaptive Mesh Refinement for Multimaterial Hydrodynamics

I. Lomov, R. Pember, J. Greenough, B. Liu

October 21, 2005

Joint Russian-American Five-Laboratory Conference on Computational Mathematics/Physics
Vienna, Austria
June 19, 2005 through June 23, 2005

Updated October 14, 2003

Patch-based Adaptive Mesh Refinement for Multimaterial Hydrodynamics

I.N. Lomov[*], R.B. Pember[*], J.A. Greenough[*], B.T. Liu[*]

[*]Lawrence Livermore National Laboratory, Livermore, CA 94550

We present a patch-based direct Eulerian adaptive mesh refinement (AMR) algorithm for modeling real equation-of-state, multimaterial compressible flow with strength. Our approach to AMR uses a hierarchical, structured grid approach first developed by (Berger and Oliger 1984), (Berger and Oliger 1984). The grid structure is dynamic in time and is composed of nested uniform rectangular grids of varying resolution. The integration scheme on the grid hierarchy is a recursive procedure in which the coarse grids are advanced, then the fine grids are advanced multiple steps to reach the same time, and finally the coarse and fine grids are synchronized to remove conservation errors during the separate advances. The methodology presented here is based on a single grid algorithm developed for multimaterial gas dynamics by (Colella et al. 1993), refined by(Greenough et al. 1995), and extended to the solution of solid mechanics problems with significant strength by (Lomov and Rubin 2003). The single grid algorithm uses a second-order Godunov scheme with an approximate single fluid Riemann solver and a volume-of-fluid treatment of material interfaces. The method also uses a non-conservative treatment of the deformation tensor and an acoustic approximation for shear waves in the Riemann solver. This departure from a strict application of the higher-order Godunov methodology to the equation of solid mechanics is justified due to the fact that highly nonlinear behavior of shear stresses is rare. This algorithm is implemented in two codes, Geodyn and Raptor, the latter of which is a coupled rad-hydro code. The present discussion will be solely concerned with hydrodynamics modeling. Results from a number of simulations for flows with and without strength will be presented.

Introduction

In this paper, we present a numerical method for solving the equations of hydrodynamics in a multi-physics AMR framework. We are concerned with computing large-deformation flows in problems consisting of multiple materials in different states. The algorithm described here is based on the treatment of the propagation of surfaces in space in terms of an equivalent evolution of volume fractions (Nichols et al. 1980), first introduced in the 1970s for representing fluid interfaces. In the present approach, the material properties are multiply valued in a cell, but the velocity is single valued (Miller and Puckett 1996). Our method embraces fluids as well as elastic-plastic solids in a single Eulerian framework. This approach is motivated by the excellent performance of Eulerian

high-order Godunov methods for single material phases. Furthermore, in the Eulerian framework adaptive mesh refinement is a relatively mature technique for dynamically applying high numerical resolution to those parts of a problem domain that require it, while solving less sensitive regions on less expensive, coarser computational grids. In combination, Eulerian high-order Godunov methods with AMR have been proven to obtain highly accurate and efficient solutions to shock capturing problems. Our implementation includes AMR capability in 3D and in parallel.

Patch based parallel AMR algorithm

The conceptual starting point for the AMR methodology development is the pioneering work of (Berger and Oliger 1984), and (Berger and Colella 1989). In this approach, a hierarchical grid structure is employed which changes dynamically in time, and is composed of logically rectangular, uniform grid "patches" of varying resolution. The solution is defined on all cells, including coarse cells which underlay cells of finer resolution. The collection of grid patches at a given resolution is referred to as a level. Patches are "properly nested" and consist of high "error" zones (defined by some refinement criteria) grouped along with some (but not many) low-error zones. Grids are dynamically created and destroyed to allow for changing features of unsteady flow. Structured grid advance achieved through use of ghost zones which are copied from neighbor patches on the same level or interpolated from the coarser level. Since we want to achieve 2nd order accurate method, linear interpolation in this process is sufficient

An explicit time-marching method of a general hierarchy of $l_{\max}$ levels of refinement can be expressed as a recursive procedure beginning with the coarsest level $l = 0$:

Recursive Procedure Advance (level l)
  if time to regrid at level $l+1$
    Estimate errors at level $l+1$
    Generate new grids at level $l+1$
    if $l+1 < l_{\max}$
      regrid $l+2$
  if $l \equiv 0$
    obtain boundary data from physical boundary conditions.
  else
    obtain boundary data from coarser grids
    and from physical boundary conditions.
  Integrate level l in time.
  if $l < l_{\max}$
    repeat r times:
      Advance (level $l+1$)
  Synchronize the data between levels l and $l+1$.
End Recursive Procedure Advance

Typically $dt_l = r\,dt_{l+1}$, where dt_l is timestep on level l, resulting in a nesting or "subcycling" of time steps for the levels in the hierarchy. We will construct the necessary interpolation, coarsening, and synchronization operators. Interlevel solution transfer operators are required when new grids are created, for the generation of boundary conditions on finer levels in the hierarchy, for synchronizing coarse and fine data in the

hierarchy, and upon the removal of refined grids. The refinement and coarsening operators presented here are designed with the following properties in mind:

1. Constant field preservation
2. 2nd order accuracy (in smooth regions)
3. Monotonicity
4. Local conservation
5. Exact inversion of refinement by coarsening

Any conservative distribution of a quantity from the coarse mesh to its corresponding fine mesh stencil may be inverted exactly with a simple summation. Once recursive timestepping on a given level is finished, the flux correction has to be applied, which changes values of coarse cells that share a face with a fine cell but are not covered by fine cells.

The implementation utilizes BoxLib (Rendleman et al. 2000), an object-oriented framework for the development of structured grid adaptive mesh refinement applications. The framework has been extended to accommodate many of the novel or unusual AMR features developed in the current work. The BoxLib framework is a C++ library, and the application code was developed using both C++ and FORTRAN, with FORTRAN being reserved for performance of critical inner loop constructs. We have found this dual language choice to be an effective paradigm for scientific calculation when the algorithms and data structures are of sufficient complexity to warrant the abstraction mechanisms provided by the C++ language.

Single material algorithm

We build our numerical scheme based on a system of conservation law type equations written in the flux form in the Eulerian frame of reference:

$$\frac{\partial U_i}{\partial t} + \nabla \cdot G_i\left(U_1,...,U_l\right) = H_i\left(U_1,...,U_l\right) \tag{1}$$

The vector U_i, $i = 1,...,l$ contains all the variables which define the state of material, the flux function G_i consists of terms which can be represented in divergent form and H_i is the source term. The first part of the system (1) is common for both fluid and solid dynamics and consists of the laws of conservation of mass, momentum and energy:

$$\frac{\partial}{\partial t}\rho + \nabla \cdot \left(\rho \mathbf{v}\right) = 0 \tag{2}$$

$$\frac{\partial}{\partial t}\left(\rho \mathbf{v}\right) + \nabla \cdot \left(\rho \mathbf{v} \otimes \mathbf{v} - \mathbf{T}\right) = 0 \tag{3}$$

$$\frac{\partial}{\partial t}\left(\rho\left(\varepsilon + \tfrac{\mathbf{v}\cdot\mathbf{v}}{2}\right)\right) + \nabla \cdot \left(\rho \mathbf{v}\left(\varepsilon + \tfrac{\mathbf{v}\cdot\mathbf{v}}{2}\right) - \mathbf{T}\cdot\mathbf{v}\right) = 0 \tag{4}$$

Advanced constitutive equations usually require integration of scalar ordinary differential equation along the particle paths:

$$\dot{F}_i = \Phi_i\left(U_1,...,U_l\right) \tag{5}$$

where $F_i, i = 1,...,l_h$ is a set of history dependent variables. Combining the equation (5)

with (1) and we can write it in a quasi-conservative form suitable for Eulerian differencing scheme:

$$\frac{\partial}{\partial t}\left(\rho F_i\right) + \nabla \cdot \left(\rho \mathbf{v} F_i\right) = \rho \Phi_i \tag{6}$$

The solid materials require an equation to evolve a deformation tensor, $\mathbf{F} = \partial \mathbf{x} / \partial \mathbf{X}$, (where $\mathbf{x}$ is the current coordinate of a material point and $\mathbf{X}$ is the initial coordinate):

$$\dot{\mathbf{F}} = \mathbf{L} \cdot \mathbf{F} \tag{7}$$

where $\mathbf{L} = \left(\nabla \cdot \mathbf{v}\right)^T$ is the velocity gradient tensor and a superposed dot denotes material time differentiation. Fortunately, a wide class of solids is elastically isotropic and can be characterized wholly by the left symmetric tensor of elastic deformations, with an evolution equation in the following form:

$$\dot{\mathbf{B}}_e = \mathbf{L} \cdot \mathbf{B}_e + \mathbf{B}_e \cdot \mathbf{L}^T - \mathbf{A}_p \tag{8}$$

where $\mathbf{A}_p$ is a plasticity operator to be defined by a constitutive model. The equation (8) is impossible to transform to form (1), unlike equation (7) (Kondaurov 1985), but in our experience we did not find any real-world application where nonconservative formulation (8) could cause any issues. Furthermore, it is convenient to separate the volumetric and deviatoric parts of $\mathbf{B}_e$, integrating them separately. The volumetric part is equivalent to equation (2). The evolution equation of the unimodular tensor $\mathbf{B}_e^{'} = \det(\mathbf{B}_e)^{-1/3}\mathbf{B}_e$ can be written in the following form:

$$\dot{\mathbf{B}}_e^{'} = \mathbf{L} \cdot \mathbf{B}_e^{'} + \mathbf{B}_e^{'} \cdot \mathbf{L}^T - \tfrac{2}{3}\mathbf{L} : \mathbf{I} - \mathbf{A}_p^{'} \tag{9}$$

Equation (9) can be converted to the form (6), treating its right part as a source term.

Once we convert the full system in the form (1), we can get its finite volume discretization by integrating in space and time for a fixed control volume ΔV and time interval Δt:

$$\int_{\Delta t} dt \int_{\Delta V} dV \left(\frac{\partial U_i}{\partial t} + \nabla \cdot G_i \right) = \int_{\Delta t} dt \int_{\Delta V} dV H_i \tag{10}$$

By applying the divergence theorem we derive a finite volume differencing scheme:

$$U_{i,\alpha}^{n+1} = U_{i,\alpha}^{n} - \Delta t \left(\nabla G\right)_{i,\alpha}^{C} + \Delta t H_i \left(U_{1,\ldots,l,\alpha}^{n,H}\right) \tag{11}$$

where the α index denotes values attributed to cell $\alpha = \{i, j, k\}$ with i, j, k being the cell coordinates in 3D index space. In order to simplify the approximation of the conservative flux term $\left(\nabla G\right)_{i,\alpha}^{C}$ and the source tern $H_i\left(U_{1,\ldots,l,\alpha}^{n+1/2}\right)$ we use the standard operator-split technique to split the update in both physical processes and space dimensions. The formal representation of such a technique is the following equation:

$$U_{i,\alpha}^{n+2} = S_H \left(S_{0,0,1} \left(S_{0,1,0} \left(S_{1,0,0} \left(S_H \left(S_{1,0,0} \left(S_{0,1,0} \left(S_{0,0,1} \left(U_{i,\alpha}^{n} \right) \right) \right) \right) \right) \right) \right) \right) \tag{12}$$

where spatially split operators

$$S_{i_\beta,j_\beta,k_\beta}\left(U^{n+m/3}_{1,\ldots,l,\alpha}\right)=U^{n+m/3}_{1,\ldots,l,\alpha}+\Delta tA_{i+1/2i_\beta,j+1/2j_\beta,k+1/2k_\beta}G_{i+1/2i_\beta,j+1/2j_\beta,k+1/2k_\beta}\left(U^{n+m/3}_{1,\ldots,l}\right)$$
$$-\Delta tA_{i+1/2i_\beta,j+1/2j_\beta,k+1/2k_\beta}G_{i+1/2i_\beta,j+1/2j_\beta,k+1/2k_\beta}\left(U^{n+m/3}_{1,\ldots,l}\right) \quad (13)$$

are applied in Strang-splitting order to keep the second-order accuracy, while the source term

$$S_H\left(U^{n,H}_{1,\ldots,l,\alpha}\right)=U^{n,H}_{1,\ldots,l,\alpha}+\Delta tV_\alpha H_\alpha\left(U^{n,H}_{1,\ldots,l,\alpha}\right) \quad (14)$$

is always applied at the end of the timestep. There are several reasons to break the formal second order accuracy of the operator splitting technique in this case. First, applying the source operator at the end of the timestep assures that we have consistent state at that time. Second, the nature of the second-order accuracy of Strang splitting is only important if operators are close to linear. For non-linear operators it is more important to keep a physically sound approximation rather than the formal order of accuracy since the split technique may give bad results in this case. The third reason is that we use the approximation of the velocity gradient $\mathbf{L}$ obtained during spatially split substeps to integrate the non-conservative equation (9). Furthermore, the source term $H_\alpha\left(U^{n,H}_{1,\ldots,l,\alpha}\right)$ can be very nonlinear and costly to calculate in the case of complicated material models, so it is beneficial to evaluate it only once per timestep. $U^{n,H}_{1,\ldots,l,\alpha}$ is defined as the state after 3 consecutive 1D sweep operators.

Let's consider an approximation of any of the 1D direction-dependent operators (13) In order to close our numerical scheme it is necessary to define a method to calculate the flux $G_{i+1/2i_\beta,j+1/2j_\beta,k+1/2k_\beta}\left(U_{1,\ldots,l}\right)$ on the edge of two cells given the $U_{1,\ldots,l}$ in some vicinity of the point α. Since this step in our dimensionally split method is one-dimensional, we will limit the description to one spatial dimension, x, with other 2 dimensions treated the same way.

The essence of the high order Godunov method which we are going to apply consists of 3 steps: calculation of slope limited derivatives of primary variables, characteristic analysis and Riemann solver. These steps are necessary to reconstruct the flux $G_{i+1/2}\left(U_{1,\ldots,l}\right)$ with high order of approximation both in space and time. First, we convert the system (1) to quasilinear form

$$\frac{\partial}{\partial t}Q+A(Q)\frac{\partial}{\partial x}Q=B(Q), \quad (15)$$

where the matrix A and vector Q have the form:

$$A = \begin{pmatrix} v_1 & \rho & & & & & & & \\ & v_1 & & & -1/\rho & & & & \\ & & v_1 & & & -1/\rho & & & \\ & & & v_1 & & & -1/\rho & & \\ & -C & & & v_1 & & & & \\ & & -G & & & v_1 & & & \\ & & & -G & & & v_1 & & \\ & \rho\eta & & & & & & v_1 & \\ & & & & & & & & v_1 \end{pmatrix}$$

$$Q = \begin{pmatrix} \rho & v_1 & v_2 & v_3 & T_{11} & T_{12} & T_{13} & \rho\varepsilon & F_i \end{pmatrix}^T \tag{16}$$

where $\eta = \varepsilon - T_{11}/\rho$ is the specific enthalpy and T_{ij} are components of Cauchy stress tensor $\mathbf{T}$. We do characteristic tracing with "frozen" right part, since it is nonlinear and could be very expensive to evaluate. Increasing the formal order of accuracy usually doesn't help to reduce errors if we have a stiff nonlinear equation and the only remedy can be increasing the number of integration points in the most cases. So we do not evaluate the right part during the stage of flux calculations. The next step is to represent matrix A in diagonal decomposition $A = S\Lambda S^{-1}$, where Λ is a diagonal matrix and S is the matrix of the right eigenvectors. The exact solution to the linearized equations (15) with "frozen" right part is

$$Q_{i+1/2}^{n+1/2} = Q_i^n + 1/2\left(\pm\Delta x I - \Delta t A\right)Q_x^n \tag{17}$$

where Q_x^n denotes $\partial Q/\partial x$ evaluated at time n, but this result includes both upwind and downwind characteristics. To make the solution fully upwind we filter the downwind characteristics from the matrix A, obtaining

$$Q_{i+1/2}^{n+1/2} = Q_i^n + 1/2\left(\pm\Delta x I - \Delta t S\Lambda^{\pm}S^{-1}\right)Q_x^n \tag{18}$$

$$\Lambda_{ii}^{\pm} = \pm\max\left(\pm\Lambda_{ii}, 0\right) \tag{19}$$

In other words, in the course of tracing to the right edge of a cell (to $x_{i+1/2} = x_i + \Delta x/2$), only those eigenvalues of A (which is evaluated at x_i) that are positive are retained. The negative eigenvalues are set to zero. Conversely, in the course of tracing to the left edge of a cell (to $x_{i+1/2} = x_i - \Delta x/2$) the positive eigenvalues of A are set to zero. The estimate of the slopes Q_x^n is very well described in the literature (Miller and Puckett 1996). We will skip this part of out method, noticing only that we are using the standard limiting differencing, slope flattening and artificial viscosity as in standard approach in gas dynamics. Since this is the "gold standard" in gas dynamics we did not feel that we need to change anything in this part of the algorithm.

Using right and left states on the cell edges computed with described characteristic tracing, we solve the Riemann problem, again using the "frozen assumption", i.e. not evaluating right part. Moreover, a general form of the source term makes the Riemann problem nonlinear, reducing the overall attractiveness of Godunov methods for system of equations where the source term or other physical processes are dominant. In many

problems of interest, the Riemann problem could be solved in self-similar approximation with satisfactory results. There are numerous papers devoted to accurate Riemann solvers in solids. Even for purely elastic materials the solution is quite complex involving multiple simple waves and jumps in longitudinal and transversal directions. In general there are two types of transversal waves, with different wavespeeds. In order to avoid this complexity and make use of the fact that in most materials transversal waves are weak, we split the solution for longitudinal and transversal mode into separate problems. A number of accurate Riemann solvers were developed over the years for gas dynamics methods. We use the standard gas dynamics approach to solve the longitudinal mode (which is converted to a pure longitudinal wave in our approximation) and an acoustic approximation to solve the transversal mode (which degenerates into a linear pure transversal wave with a unique transversal velocity). Let's denote a set of primitive variables on the left side of the cell edge as Q^L and on the right side as Q^R. Velocity and stress on the contact discontinuity are calculated as:

$$\begin{aligned} v_1^* &= \left(\rho^L c_l^L v_1^L + \rho^R c_l^R v_1^R - \left(T_{11}^L - T_{11}^R\right)\right) / \left(\rho^L c_l^L + \rho^R c_l^R\right) \\ T_{11}^* &= \left(\rho^L c_l^L T_{11}^R + \rho^R c_l^R T_{11}^L - \rho^L c_l^L \rho^R c_l^R \left(v_1^L - v_1^R\right)\right) / \left(\rho^L c_l^L + \rho^R c_l^R\right) \end{aligned} \tag{20}$$

While other, more accurate Riemann solvers exist, (20) gives satisfactory results in most practical problems and improved accuracy doesn't justify the increased cost of transcendental or iterative Riemann solvers.

The tangential state of the contact discontinuity is calculated in a similar way:

$$\begin{aligned} v_2^* &= \left(\rho^L c_t^L v_2^L + \rho^R c_t^R v_2^R - \left(T_{12}^L - T_{12}^R\right)\right) / \left(\rho^L c_t^L + \rho^R c_t^R\right) \\ T_{12}^* &= \left(\rho^L c_t^L T_{12}^R + \rho^R c_t^R T_{12}^L - \rho^L c_t^L \rho^R c_t^R \left(v_2^L - v_2^R\right)\right) / \left(\rho^L c_t^L + \rho^R c_t^R\right) \\ v_3^* &= \left(\rho^L c_t^L v_3^L + \rho^R c_t^R v_3^R - \left(T_{13}^L - T_{13}^R\right)\right) / \left(\rho^L c_t^L + \rho^R c_t^R\right) \\ T_{13}^* &= \left(\rho^L c_t^L T_{13}^R + \rho^R c_t^R T_{13}^L - \rho^L c_t^L \rho^R c_t^R \left(v_3^L - v_3^R\right)\right) / \left(\rho^L c_t^L + \rho^R c_t^R\right) \end{aligned} \tag{21}$$

Based on the sign of v_1^* we define an initial state:

$$Q^I = \begin{cases} Q^L, & v_1^* > 0 \\ Q^R, & v_1^* \le 0 \end{cases} \tag{22}$$

Then we estimate longitudinal sound speed at the interface:

$$c_l^* = c_l^I \sqrt{1 + \left(\partial C / \partial T_{11}\right)_s^I \left(T_{11}^* - T_{11}^I\right)} \tag{23}$$

and calculate the density and energy change due to the longitudinal wave:

$$\begin{aligned} \rho^* &= \rho^I - \left(T_{11}^* - T_{11}^I\right) \Big/ \left(\max\left(c_l^I, c_l^*\right)\right)^2 \\ \varepsilon^* &= \varepsilon^I \, \rho^* / \rho^I - \left(\rho^* / \rho^I - 1\right)\left(T_{11}^* + T_{11}^I\right) / 2 \end{aligned} \tag{24}$$

Once we have found the state at the contact discontinuity, we interpolate between it and the initial state to find the state at the $x = \text{const}$ line. First, we calculate characteristic

speeds:

$$\begin{aligned} s^I &= c^I - \operatorname{sign}\left(v^*\right)v^I \\ s^* &= c^* - \left|v^*\right| \end{aligned} \tag{25}$$

The weights of interpolation are calculated assuming that we have a shock wave if $T_{11}^* < T_{11}^I$:

$$f = \begin{cases} 1, & \left(s^I + s^*\right)/2 > 0 \\ 0, & \left(s^I + s^*\right)/2 \le 0 \end{cases} \tag{26}$$

and rarefaction fan otherwise.

$$f = \max\left(\min\left(\tfrac{1}{2}\left(1 + \left(s^I + s^*\right)\Big/\left(s^I - s^*\right)\right), 1\right), 0\right) \tag{27}$$

The values of stress, velocity, density and internal energy at the cell edges are given by the following formulas:

$$\begin{aligned} T_{11}^g &= fT_{11}^* + \left(1-f\right)T_{11}^I, \\ v_1^g &= fv_1^* + \left(1-f\right)v_1^I, \\ \rho^g &= f\rho^* + \left(1-f\right)\rho^I, \\ \varepsilon^g &= f\varepsilon^* + \left(1-f\right)\varepsilon^I \end{aligned} \tag{28}$$

After reconstructing the Godunov state $U_{1,\ldots,l}^g$ we can calculate fluxes between cells $G_{i+1/2i_\beta, j+1/2j_\beta, k+1/2k_\beta}\left(U_{1,\ldots,l}\right)$ and complete the single material algorithm.

Mixed cell treatment

The biggest challenge in the Eulerian and multimaterial ALE methods is the treatment of mixed cells which contain several materials. The algorithm described here treats the propagation of surfaces in space in terms of an equivalent evolution of volume fractions defined by the equation:

$$\begin{aligned} &\frac{\partial f_\alpha}{\partial t} + \nabla\cdot\left(f_\alpha \mathbf{v}\right) = \frac{f_\alpha}{K_\alpha} K \nabla\cdot\mathbf{v} \\ &1/K = \sum f_\alpha / K_\alpha \end{aligned} \tag{29}$$

where f_α and K_α are the volume fraction and bulk modulus of each material α. The approach to modeling multimaterial cells is similar to that in (Miller and Puckett 1996). Specifically, material properties have multiple values in a cell, but the velocity and stress are single valued. In order to use the single-fluid solver it is necessary to define an effective single phase for the mixed cells and to update material volume fractions based on self-consistent cell thermodynamics:

$$
\begin{aligned}
1/K &= \sum f_\alpha / K_\alpha \\
1/G &= \sum f_\alpha / G_\alpha \\
T_{ii} &= 1/K \sum f_\alpha T_{ii\alpha} / K_\alpha \\
T_{ij,i\neq j} &= 1/G \sum f_\alpha T_{ij\alpha} / G_\alpha
\end{aligned}
\tag{30}
$$

where $G_\alpha, T_{ij\alpha}$ are the shear modulus and stress tensor components of material α. Distribution of the velocity gradient amongst each material in the cell required to integrate (18) for each material is done in a similar way:

$$\mathbf{L}_\alpha = \mathbf{L} G / G_\alpha \tag{31}$$

In order to advect volume fractions we use a high order interface reconstruction (interface tracking), which preserves linear interfaces during translation. In order to adjust for the non-conservative right part of (29) and satisfy the constraint on volume fraction $\sum f_\alpha = 1$ we compress the advected volumes proportionally to compressibility of each material. The further adjustment is based on the assumption of fast equilibration of partial pressures in the cell. The pressure relaxation algorithm is used. The algorithm consists of iterative adjustments of volume fractions. First, average pressure is calculated:

$$p = \frac{\sum_\alpha f^\alpha p^\alpha / K^\alpha}{\sum_\alpha f^\alpha / K^\alpha} \tag{32}$$

Next, the change of volume fraction for current iteration step is calculated:

$$\delta f_\alpha = \beta_\alpha f_\alpha \left(p^\alpha - p \right) \Big/ K^\alpha \tag{33}$$

The limiter β_a is chosen from numerical and physical considerations, i.e. the resulting volume fraction should within (0:1) range, there should be enough time for waves to travel within the cell, etc. There is no stringent requirement for pressure relaxation process to converge completely, since sometimes it is divergent and it is important only for quasistatic processes, where there are enough timesteps to establish equilibrium.

Constitutive equations

In contrast with standard approaches to plasticity which introduce measures of inelastic deformation through evolution equations, the approach taken here is to propose evolution equations directly for elastic deformation measures (Rubin et al. 2000). Specifically, within the context of the proposed algorithm it is convenient to introduce a measure of elastic deformation as a symmetric, invertible, positive definite tensor Be which is determined by integrating the evolution equation (8). The tensor $\mathbf{A}_p$ includes the inelastic effects of the rate of plastic deformation as well as that due to tensile failure and compaction. For porous materials it is common to introduce the current value ϕ of porosity, its reference value Φ, and the reference density ρ_{s0} of the solid matrix, such that

$$J_e = \frac{1-\phi}{1-\Phi} J, \quad \rho_0 = (1-\Phi)\rho_{s0}, \qquad \rho = (1-\Phi) J_e^{-1} \rho_{s0} \tag{34}$$

The Helmholtz free energy ψ is assumed to be a function of the variables, $J_e, \mathbf{B}_e^{'}$ and temperature θ. However, since ψ must remain unaltered under superposed rigid body motions it follows that it can be a function of $\mathbf{B}_e^{'}$ only through its two independent invariants $\alpha_1 = \mathbf{B}_e^{'} : \mathbf{I}$, $\alpha_2 = \mathbf{B}_e^{'} : \mathbf{B}_e^{'}$. For simplicity, ψ is taken to be independent of α_2 so that it takes the form $\psi = \hat{\psi}(J_e, \alpha_1, \theta)$.

Constitutive equations are required to satisfy statements of the second law of thermodynamics which include the condition that heat flows from hot to cold, and the condition that the material dissipation is nonnegative:

$$\mathbf{T} : \mathbf{D} - \rho(\dot{\psi} + \eta\dot{\theta}) \geq 0, \tag{35}$$

where $\mathbf{D} = (\mathbf{L} + \mathbf{L}^{\mathrm{T}})/2$, and η is specific entropy. For the model under consideration, the Cauchy stress $\mathbf{T}$ and the entropy η. are given in the hyperelastic forms:

$$\begin{aligned} \mathbf{T} &= -p\mathbf{I} + \mathbf{T}^{'}, \qquad p = -\rho J_e \, \partial\psi / \partial J_e, \\ \mathbf{T}^{'} &= 2\rho \mathbf{B}_e^{''} \, \partial\psi / \partial \alpha_1, \qquad \eta = -\partial\psi / \partial\theta \end{aligned} \tag{36}$$

and can be related to pressure p_s and deviatoric stress $\mathbf{T}_s^{'}$ of the solid matrix:

$$\begin{aligned} p &= (1-\phi) p_s, \qquad \mathbf{T}^{'} = (1-\phi)\mathbf{T}_s^{'}, \\ p_s &= -\rho_{s0} \, \partial\psi / \partial J_e, \quad \mathbf{T}^{'} = 2J_e^{-1}\rho_{s0}\mathbf{B}_e^{''} \, \partial\psi / \partial \alpha_1 \end{aligned} \tag{37}$$

In particular, the Helmholtz free energy ψ_s of a nonporous matrix is specified by:

$$\rho_{s0}\psi = \rho_{s0}\hat{\psi}_1(J_e, \theta) + 1/2\,\hat{G}(J_e, \theta)(\mathbf{B}_e^{'} : \mathbf{I} - 3) \tag{38}$$

where $\hat{G}(J_e, \theta)$ is shear modulus

Next, the inelastic deformation tensor $\mathbf{A}_p$ is separated into a part $\mathbf{A}_p^{'}$ associated with viscoplasticity and a part $\mathbf{A}_v$ associated with void formation (due to porosity and cracks) and compaction:

$$\mathbf{A}_p = \mathbf{A}_p^{'} + \mathbf{A}_v, \qquad \mathbf{A}_p^{'} = \Gamma_p \left(\mathbf{B}_e^{'} - \left(\frac{3}{\mathbf{B}_e^{'} : \mathbf{I}} \right) \mathbf{I} \right), \qquad \mathbf{A}_v = \Gamma_v \mathbf{I} \tag{39},$$

where the scalar rate functions Γ_p, Γ_v require constitutive equations.

This framework of porosity and general plasticity models allows us to use very general constitutive equations for solid matrix pressure p_s based on a wide-range of equations of state to specify $\hat{\psi}\left(J_e,\theta\right)$, shear modulus $\hat{G}\left(J_e,\theta\right)$ and rate functions. It is possible to prove that appropriate choice of these dependencies will satisfy the second law of thermodynamics. A complete description of the specific constitutive relations is beyond the scope of this paper and can be found in (Rubin, Vorobiev et al. 2000), (Rubin and Lomov 2003), (Lomov et al. 2005), (Liu et al. 2005). The rate-dependent formulation (39) can be easily converted to the well-known yield function from, which depends on strain rate and includes plastic strain and pressure hardening, Löde angle dependence, thermal and structural softening. A void evolution equation can describe initial porosity compaction with shear enhancement, spall, directional tensile failure, dilatancy under positive pressure (bulking).

Simulations

1D test: motion of a metal plate in air

In order to test the multimaterial algorithm described in this paper we calculated a simple problem which has large density differences and strong shocks. This combination proves to be very difficult to calculate with direct Eulerian methods. At $t=0$ the metal plate starts to move with velocity of 2 kilometers per second in very cold air at ambient conditions. Since initial specific internal energy of gas is significantly smaller then specific internal energy, it is extremely important to preserve the energy balance and keep the gas internal energy positive. Figure 1 shows profiles of density, pressure, energy and

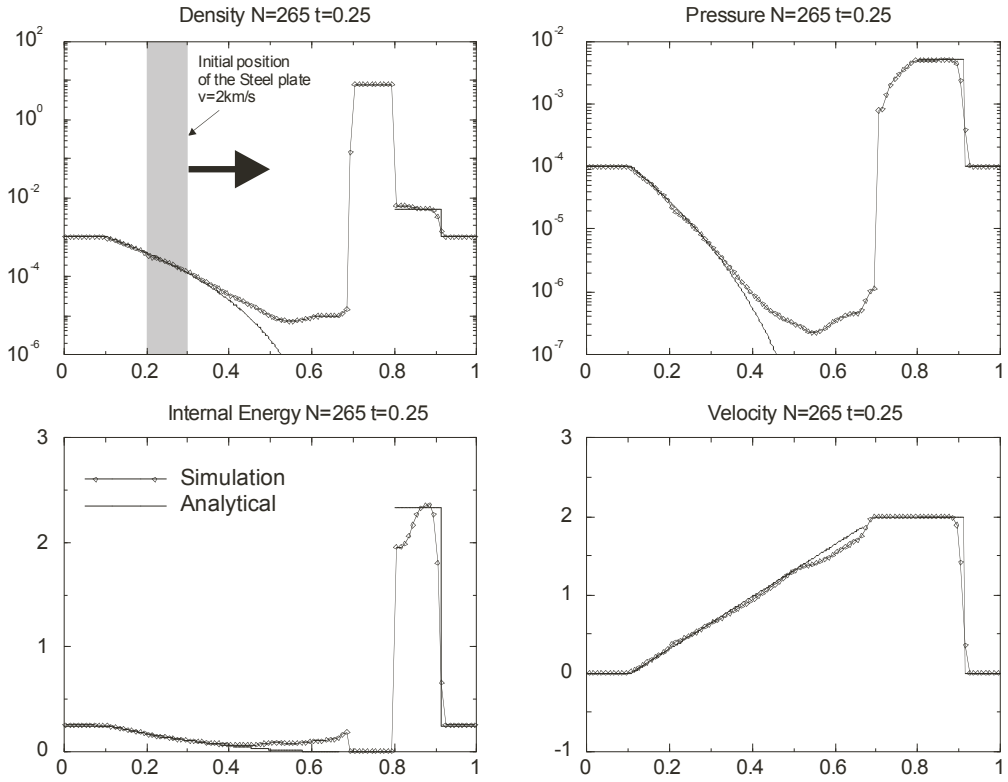

Figure 1. 1D test of multimaterial algorithm.

velocity after 265 timesteps. We see good agreement of the simulation results with analytical profiles. The internal energy in the gas is within physically justified limits. Note that the velocity of the plate is higher than the velocity of gas expansion into vacuum, so vacuum region should form behind the metal plate. Since out algorithm doesn't allow vacuum cells, we see that cells behind the metal plate are filled with gas, but the density of material is extremely low (2-3 order of magnitude lower then initial density).

Spherical wave propagation test in marble

Here we demonstrate extensive capabilities for simulation of complex material response within the AMR framework. We applied a directional tensile failure model (Rubin and Lomov 2003) in a calculation of an experiment of the dynamic fracture of a marble cylinder (Antoun and Curran 1996)

The model was calibrated using laboratory data that included elastic properties, unconfined compressive strength, and a pressure dependent failure surface. Pressure-volume data from 1D strain wave propagation experiments were also used to calibrate the Mie-Grüneisen EOS used in the simulations. Material parameters that could not be determined from the aforementioned data were determined through an optimization process using the measured particle velocity histories shown earlier in Fig 2. As shown in the figure, the calibrated model is in good agreement with the data at early time, when the flow field can be reasonably viewed as spherically symmetric. At late time, reflected waves from the cylindrical boundary of the specimen converge toward the charge cavity and in so doing render the flow field three-dimensional. Also at late time, the sample response becomes anisotropic due to the interaction of the stress waves with pre-existing planes of weakness in the sample. These two phenomena cause a breakdown in the 2D axisymmetry assumption. For this reason no attempt was made to match the late time velocity histories.

The damage patterns computed with the calibrated model are shown in Fig. 2. The two halves of the figure show void volume fraction and crack patterns, both of which are

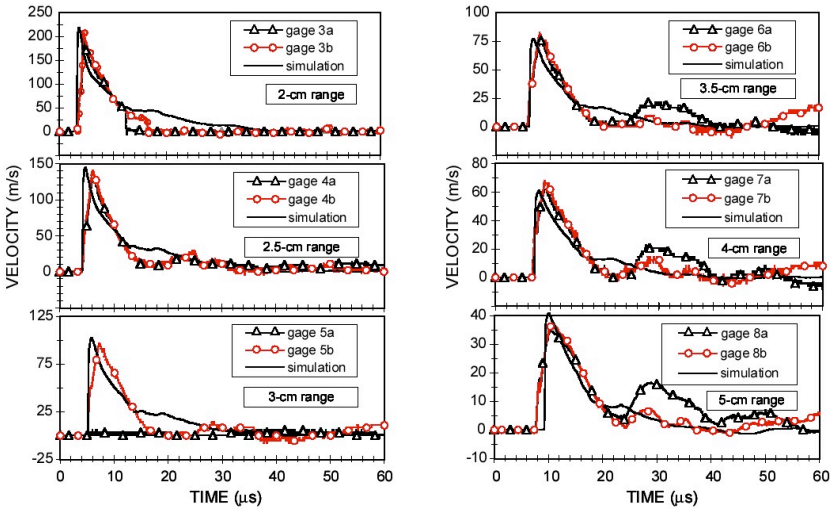

Figure 2. Measured and simulated particle velocity histories at 6 radii from the explosive charge.

indication of damage. The main difference between the two is that void volume fraction is reversible (i.e., voids can undergo recompaction under compression) whereas damage is irreversible, increasing under tension and remaining constant under compression.

These patterns look remarkably similar to the cracking patterns observed in the experiment. Like in the experiment, two crack networks are observed; the first consisting of radial cracks propagating away from the charge cavity toward the free surface, and the second consisting of rings of circumferential cracks caused by the reflected wave near the free surface of the specimen. The simulated circumferential cracks network is closer to the surface of the specimen than was observed experimentally. This is probably because in the simulation the reflected wave is spherically symmetric, and therefore more intense than its cylindrically symmetric counterpart in the experiment.

Fig. 3 also shows a near-source region dominated by bulking. Bulking porosity as high as 10% was computed in the near-source region. This form of isotropic scalar damage is related to plastic distortion under compression. It is different in nature from the radial and circumferential components of the directional damage variable.

The 2D simulations are in reasonably good agreement with the data indicating that our multidimensional cracking model is well suited for simulating directional damage within a continuum mechanics framework. To improve agreement with data, a 3D simulation is needed to properly account for specimen geometry, including preexisting joints, and for the complex wave interactions that take place during the later stages of the experiment.

Conclusions

We have presented a software framework, a numerical algorithm and constitutive equations for integration of multimaterial Euler equations for solids, fluids and gases. We integrate conservation laws, a transport equation for volume of each material, an equation for evolution elastic deformations and a number of kinetic equations for internal state variables. The fundamental assumption underlying this approximation is that in a cell that

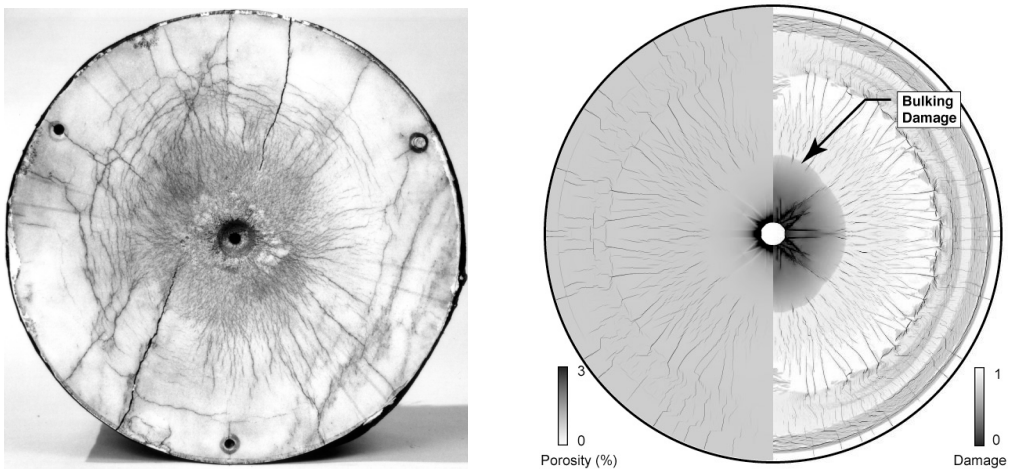

Figure 3. Observed damage at the midsection of the explosively loaded Danby marble specimen (left). Void volume and directional damage from the 2D simulation of the spherical wave experiment (right).

contains more then one material, the pressure and velocity are single valued. The resulting system is hyperbolic and can be solved with a high order Godunov method. The single phase solver retains all the properties of the well-established gas dynamics Godunov method, with necessary modifications to take into account full stress tensor. The use of AMR allows us to focus the majority of the computational effort on regions with interfaces between materials and regions with steep pressure and density changes. The methodology presented here provides efficient and effective dynamic approach and achieves acceptable load balance for AMR grids. The entire software system, both base and framework libraries, as well as applications software and physics algorithms, has been optimized for efficient use of modern large-scale parallel computing platforms.

Acknowledgements

This work was performed under the auspices of the U.S. Department of Energy by the University of California Lawrence Livermore National Laboratory under contract No. W-7405-Eng-48.

References

Antoun, T. A. and D. R. Curran (1996). Wave Propagation in Intact and Jointed Calcium Carbonate (CaCO3) Rock.

Berger, M. J. and P. Colella (1989). "Local Adaptive Mesh Refinement for Shock Hydrodynamics." Journal of Computational Physics **82**(1): 64-84.

Berger, M. J. and J. Oliger (1984). "Adaptive Mesh Refinement for Hyperbolic Partial-Differential Equations." Journal of Computational Physics **53**(3): 484-512.

Colella, P., H. M. Glaz and R. E. Ferguson (1993). Multi-Fluid Algorithms for Eulerian Finite Difference Methods, Unpublished Manuscript.

Greenough, J. A., V. E. Beckner, R. B. Pember, W. Y. Crutchfield, J. B. Bell and P. Colella (1995). An Adaptive Multifluid Interface-Capturing Method for Compressible Flow in Complex Geometries. 26th AIAA Fluid Dynamics Conference, San Diego, CA.

Kondaurov, V. I. (1985). "Relaxation-Type Equations for Viscoelastic Media with Finite Deformations." Pmm Journal of Applied Mathematics and Mechanics **49**(5): 608-615.

Liu, B. T., I. Lomov and O. Y. Vorobiev (2005). Simulation of Shock Loading in Saturated Geologic Materials. International Symposium on Plasticity, Kauai, HI, United States.

Lomov, I. and M. B. Rubin (2003). "Numerical simulation of damage using an elastic-viscoplastic model with directional tensile failure." Journal De Physique Iv **110**: 281-286.

Lomov, I., O. Y. Vorobiev and T. H. Antoun (2005). Simulation of shock wave propagation and damage in geologic materials. International Symposium on Plasticity, Kauai, HI, United States.

Miller, G. H. and E. G. Puckett (1996). "A high-order Godunov method for multiple condensed phases." Journal of Computational Physics **128**(1): 134-164.

Nichols, B. D., C. W. Hirt and R. S. Hotchkiss (1980). SOLA-VOF: a solution algorithm for transient fluid flow with multiple free boundaries. Washington, D.C., U.S. Government Printing Office.

Rendleman, C. A., V. E. Beckner, M. Lijewski, W. Crutchfield and J. B. Bell (2000). "Parallelization of structured, hierarchical adaptive mesh refinement algorithms." Computing & Visualization in Science **3**(3): 147-57.

Rubin, M. B. and I. Lomov (2003). "A thermodynamically consistent large deformation elastic-viscoplastic model with directional tensile failure." International Journal of Solids and Structures **40**(17): 4299-4318.

Rubin, M. B., O. Y. Vorobiev and L. A. Glenn (2000). "Mechanical and numerical modeling of a porous elastic-viscoplastic material with tensile failure." International Journal of Solids and Structures **37**(13): 1841-1871.